Nigerian Journal of Physics (NJP)
ISSN online: 3027-0936
ISSN print: 1595-0611
DOI: https://doi.org/10.62292/njp.v35i1.2026.513
Volume 35(1), March 2026

Monte Carlo Dosimetric Evaluation of Bismuth Oxide/Barium Sulfate–Epoxy Grid Block Collimators for Spatially Fractionated Radiotherapy

***[1]Oluniyi Samuel Makinde, [2]Abiodun Emmanuel Oni, [1]Olaosebikan Akanni Aremu, [2]Adewale Abraham Aremu and [2]Olatunde Michael Oni**

[1]Department of Physics, The Polytechnic, Ibadan, Nigeria
[2]Department of Pure and Applied Physics, Ladoke Akintola University of Technology, Ogbomoso, Nigeria

*Corresponding authors' email: samuelmakinde566@gmail.com

Keywords:
Spatially Fractionated radiotherapy,
GRID Therapy,
Monte Carlo Simulation,
TOPAS,
Polymer composite,
Bismuth Oxide,
Peak-to-Valley Dose Ratio,
Radiation Dosimetry.

ABSTRACT

This study evaluates the dosimetric performance of Bi_2O_3/$BaSO_4$–epoxy composite grid block collimators for Spatially Fractionated Radiotherapy (SFRT) as lightweight, non-toxic alternatives to conventional brass and Cerrobend grids in LINAC-based treatments. Epoxy composites reinforced with Bi_2O_3 and $BaSO_4$ were synthesized and machined into clinically realistic grid geometries. Experimental linear and mass attenuation coefficients were measured at therapeutic photon energies and validated against the NIST XCOM database. Monte Carlo simulations were performed using TOPAS to model a 6 MV TrueBeam LINAC with a 22 × 22 × 7.5 cm^3 grid block containing hexagonally arranged divergent circular apertures. Percentage Depth Dose (PDD), lateral dose profiles, surface dose, and Peak-to-Valley Dose Ratio (PVDR) were evaluated in a water phantom and compared with brass and Cerrobend grids. The composite reproduced PDD within ±5% of BJR 25 reference data, with $d_{max} \approx 1.5$ cm for all materials. Surface dose was slightly higher than Cerrobend (+2.53%) and brass (+1.23%) but remained clinically acceptable. At 10 cm depth, PVDR values were 4.04 (composite), 4.13 (brass), and 4.78 (Cerrobend). Beam profiles were symmetric, and measured attenuation coefficients showed strong agreement with XCOM predictions ($R^2 > 0.99$). These results indicate that Bi_2O_3/$BaSO_4$–epoxy composite grid blocks achieve dosimetric performance comparable to conventional metallic grids and are suitable for SFRT applications.

INTRODUCTION

Radiotherapy remains a cornerstone of contemporary cancer management, contributing substantially to tumor control and survival across a wide range of malignancies (Abdel-Wahab *et al*., 2013; Khan and Gibbons, 2014). Advances in beam delivery, treatment planning, and dosimetric verification have significantly improved dose conformity and normal tissue sparing; however, treatment-related toxicity, infrastructure cost, and limited access to advanced technologies continue to pose major challenges, particularly in low- and middle-income countries (LMICs) (Barton *et al*., 2014; Rosenblatt et al., 2013; Zubizarreta *et al*., 2015). These challenges have renewed interest in alternative radiotherapy techniques capable of delivering high therapeutic doses while maintaining acceptable tolerance in normal tissue.

Spatially Fractionated Radiotherapy (SFRT), commonly referred to as GRID therapy, is a technique in which a spatially modulated radiation field delivers high-dose regions (peaks) separated by low-dose regions (valleys), thereby exploiting differential biological responses in tumor and normal tissues (Harrington et al., 2011; Mohiuddin *et al*., 1999). Clinical and experimental studies have demonstrated that SFRT can achieve tumor control with reduced toxicity in bulky, radioresistant, or advanced tumors where conventional uniform irradiation may be ineffective (Huhn *et al*., 2006; Prezado *et al*., 2017). The therapeutic effectiveness of SFRT is strongly influenced by the quality of spatial dose modulation, typically quantified using parameters such as Percentage Depth Dose (PDD), lateral beam profiles, and the Peak-to-Valley Dose Ratio (PVDR) (Huhn *et al*., 2006; Meigooni *et al*., 2002).

Central to SFRT delivery is the grid block collimator, which spatially modulates the photon beam through an array of regularly arranged apertures. Traditionally, grid

blocks have been fabricated from high-density metallic materials such as Cerrobend and brass due to their favorable attenuation properties and ease of machining (Taherkhani *et al*., 2010; Tellili *et al*., 2017). Despite their clinical utility, these materials present significant limitations, including high weight, toxicity associated with lead-containing alloys, mechanical handling challenges, and restricted availability in resource-limited settings (Belgin and Aycik, 2015; McCaffrey *et al*., 2007). These drawbacks have motivated increasing interest in developing alternative, lead-free materials for radiation collimation and shielding.

Polymer-based composites reinforced with high atomic number fillers have emerged as promising candidates for radiation shielding applications, offering a combination of effective photon attenuation, reduced toxicity, and improved manufacturability (Harish *et al*., 2012; Nambiar and Yeow, 2012; More *et al*., 2021). Among these materials, epoxy matrices filled with bismuth oxide (Bi_2O_3) and barium sulfate ($BaSO_4$) have attracted particular attention due to their high atomic numbers, favorable photoelectric absorption characteristics, and chemical stability (Ambika *et al*., 2016; Hemavathi *et al*., 2023; Zare *et al*., 2014). Experimental and computational investigations have consistently shown that increasing filler loading in such composites enhances linear and mass attenuation coefficients, reduces photon transmission, and improves lead-equivalent performance across diagnostic and therapeutic photon energies (Mann & Agarwal, 2023; Poltabtim *et al*., 2018; Turhan *et al*., 2023).

Although the radiation shielding properties of Bi_2O_3- and $BaSO_4$-filled polymer composites are well documented, their application as grid block collimators for megavoltage SFRT remains relatively unexplored. SFRT places stringent dosimetric demands on collimator materials, including stable peak and valley dose formation, reproducible depth–dose behavior, clinically acceptable surface dose, and sufficient PVDR at therapeutic depths (Huhn *et al*., 2006; Prezado *et al*., 2017). Accurate evaluation of these parameters is challenging using experimental techniques alone due to steep dose gradients and complex geometries. Consequently, Monte Carlo simulation methods have become the reference standard for SFRT dosimetric assessment, offering high-fidelity modeling of photon transport, beam–matter interactions, and material heterogeneity (Clementel *et al*., 2015; Verhaegen and Seuntjens, 2003).

In this study, a comprehensive Monte Carlo dosimetric evaluation of synthesized Bi_2O_3/$BaSO_4$–epoxy composite grid block collimators is performed for LINAC-based SFRT. Clinically realistic grid block geometries incorporating hexagonally arranged divergent apertures are modeled under a 6 MV photon beam and benchmarked against conventional brass and Cerrobend grids. Experimental attenuation properties of the composite materials are first validated against reference photon interaction data from the NIST XCOM database (Berger *et al*., 2010; Hubbell & Seltzer, 1995). Key dosimetric parameters—including PDD, lateral beam profiles, surface dose, and PVDR—are then evaluated in a water phantom using Monte Carlo simulations. By directly comparing composite and metallic grid blocks under identical irradiation conditions, this work aims to establish the feasibility of lightweight, non-toxic polymer composites as clinically viable alternatives for SFRT, with particular relevance for expanding access to advanced radiotherapy techniques in resource-constrained environments.

MATERIALS AND METHODS

Composite Synthesis, Molding, and Sample Preparation (shortened)

Epoxy-based composites were prepared using a bisphenol-A epoxy resin matrix and high-purity Bi_2O_3 and $BaSO_4$ powders selected for lead-free photon attenuation (Ambika *et al*., 2016; Harish *et al*., 2012; Zare *et al*., 2014). The formulation was fixed at 60 wt% total filler (40 wt% Bi_2O_3, 20 wt% $BaSO_4$) with the remaining 40 wt% comprising the epoxy resin and curing system. Fillers were oven-dried (105 °C, 12 h) before incorporation into epoxy. Dispersion was achieved by mechanical mixing (800 rpm, 20 min) followed by ultrasonication (40 kHz, 15 min) to reduce agglomeration (Poltabtim *et al*., 2018; Nambiar and Yeow, 2012; Mann and Agarwal, 2023). After addition of curing agent (gentle mixing, 5 min), the slurry was cast into precision molds corresponding to standard SFRT grid block geometries with hexagonally packed, divergent circular apertures (Huhn *et al*., 2006; Powers *et al*., 1973). Samples were cured at 25 ± 2 °C for 24 h and post-cured at 60 °C for 4 h (Hemavathi et al., 2023), then demolded and lightly machined to meet accessory-tray tolerances. Composite density was 2.85 ± 0.03 g·cm^{-3} (Archimedes) and Shore-D hardness was 78 ± 2 (mean ±1 SD, n = 3), indicating substantially reduced mass relative to brass and Cerrobend and sufficient mechanical robustness for handling and mounting (McCaffrey *et al*., 2007; Tellili *et al*., 2017; More *et al*., 2021).

Experimental Determination of Attenuation Coefficients

The attenuation properties of the synthesized Bi_2O_3/$BaSO_4$–epoxy composite were experimentally evaluated to provide benchmark data for Monte Carlo simulations. Measurements were conducted using a narrow-beam transmission geometry to minimize scattered radiation and ensure accurate photon interaction parameters (Hubbell, 2006; Knoll, 2010).

Monoenergetic gamma-ray photons were obtained from calibrated point sources. The setup comprised a

collimated source, composite sample, and NaI(Tl) scintillation detector coupled to a multichannel analyzer (MCA), aligned along a common axis. Energy calibration was performed using standard reference sources prior to measurements (Knoll, 2010; Akkurt et al., 2005).

For each energy, transmitted intensity I through a sample of thickness x was measured and compared with incident intensity I_0. The linear attenuation coefficient (μ) was calculated using the Beer–Lambert law (Eq. 1):

$$I = I_0 \exp(-\mu t) \quad (1)$$

The mass attenuation coefficient (μ_m) was obtained from (Eq. 2) :

$$\mu_m = {}^{\mu}/_{\rho} \quad (2)$$

where ρ is the measured composite density. Experimental $\mu_m$values were compared with NIST XCOM data to validate material composition for Monte Carlo modeling (Berger *et al*., 2010; Hubbell and Seltzer, 1995).

Each measurement was performed in triplicate, and background-corrected photopeak counts were averaged. Counting times ensured statistical uncertainties below 2% across all energies (Akkurt *et al*., 2005; Latha *et al.,* 2012).

Uncertainty Analysis

Uncertainty in the experimentally determined attenuation coefficients arises from photon counting statistics, sample thickness measurement, density determination, and instrumental stability. The combined relative uncertainty in the linear attenuation coefficient (μ) was evaluated using standard error propagation (Eq. 3) (Attix, 2004; Taylor, 1997):

$$\frac{\Delta\mu^2}{\mu} = \frac{\Delta I^2}{I} + \frac{\Delta {I_0}^2}{I_0} + \frac{\Delta x^2}{x} \quad (3)$$

where ΔI and ΔI_0 denote uncertainties in transmitted and incident photon intensities (dominated by counting statistics), and Δx represents the uncertainty in sample thickness (±0.01 mm). For mass attenuation coefficients (MAC), density uncertainty (Δρ), determined via the Archimedes method, was additionally included.

The overall expanded uncertainty (k = 1) in MAC values was within 3–5%, consistent with comparable polymer composite studies (Manjunatha *et al*., 2017; Obaid *et al*., 2018). Linear regression analysis between experimental and XCOM-predicted MAC values yielded $R^2 > 0.99$, confirming the reliability of the measurements. These validated attenuation coefficients were subsequently implemented in the TOPAS Monte Carlo framework to ensure consistency between experimental shielding performance and simulated dose distributions for SFRT grid block evaluation

Monte Carlo Modeling of LINAC and Grid Block Geometry and Dosimetric Scoring Using TOPAS

Monte Carlo simulations were performed using the Tool for Particle Simulation (TOPAS), a Geant4-based application specifically developed for radiotherapy and medical physics research. TOPAS provides high-precision modeling of particle transport, beam delivery systems, and complex geometries, making it particularly suitable for Spatially Fractionated Radiotherapy (SFRT) dosimetric evaluations (Perl *et al*., 2012; Verhaegen and Seuntjens, 2003).

LINAC Beam Modeling

A clinical 6 MV photon beam from a Varian TrueBeam linear accelerator was modeled in TOPAS following published and validated accelerator head configurations. The LINAC model included the primary electron source incident on a tungsten target, primary collimator, flattening filter, monitor chambers, and secondary collimation system. Electron beam parameters—mean energy, energy spread, and focal spot size—were tuned iteratively to reproduce reference Percentage Depth Dose (PDD) and lateral dose profiles for a standard 10 × 10 cm² open field in water (Bedford *et al*., 2019; Verhaegen & Seuntjens, 2003).

Beam validation was carried out by comparing simulated depth–dose curves and lateral profiles against BJR 25 reference data, ensuring agreement within ±5% across clinically relevant depths and field sizes. Once validated, the same beam model was used consistently for all grid block simulations to allow direct material-based comparisons.

Grid Block Geometry Modeling

The SFRT grid block was modeled as a solid rectangular structure with dimensions of 22 × 22 × 7.5 cm³, positioned in the accessory tray location upstream of the water phantom, consistent with clinical grid therapy setups. The grid block contained a hexagonally packed array of divergent circular apertures, designed to reproduce standard SFRT geometrical specifications reported in the literature (Huhn *et al*., 2006; Powers *et al*., 1973).

At the upstream surface, apertures had a nominal diameter of 0.6 cm with a center-to-center spacing of 1.14 cm, and were linearly diverged toward the downstream surface to preserve beam divergence and maintain geometric field fidelity at depth. Three grid block materials were modeled independently: Cerrobend, brass, and the synthesized Bi_2O_3/$BaSO_4$–epoxy composite. Material definitions for the composite grid block were derived directly from experimentally measured density and elemental composition, with photon interaction cross sections validated against NIST XCOM data (Berger *et al*., 2010).

Phantom Geometry and Simulation Parameters

A water phantom (40 × 40 × 40 cm³) was positioned at a source-to-surface distance (SSD) of 100 cm, following standard dosimetric practice. The phantom was discretized using a three-dimensional Cartesian scoring grid with voxel dimensions of 1 × 1 × 1 mm³ in high-gradient regions beneath the grid block and coarser

resolution outside the modulated field to optimize computational efficiency.

Photon and secondary electron transport cutoffs were set to 0.1 mm, and electromagnetic physics processes were modeled using the Geant4 standard electromagnetic physics list, suitable for megavoltage photon simulations (Allison *et al*., 2016). For each simulation scenario, at least 1×10^8 primary photon histories were tracked to achieve statistical uncertainties below 2% (1σ) in both peak and valley dose regions.

Dosimetric Scoring and Evaluation Metrics

Dose deposition within the water phantom was scored as absorbed dose to water using the built-in TOPAS dose scorers. Percentage depth dose (PDD) was evaluated along the central beam axis beneath peak regions and normalized to the maximum dose. Lateral dose profiles were extracted at clinically relevant depths, including the surface, depth of maximum dose (d_{max}), and 10 cm, to quantify peak–valley structure, symmetry, and spatial modulation. The peak-to-valley dose ratio (PVDR) was calculated as the ratio of the mean dose in peak regions to that in adjacent valley regions at the same depth and was used as a principal metric of SFRT modulation quality (Huhn et al., 2006; Prezado et al., 2017). Surface dose was determined at the phantom entrance plane to assess material-dependent buildup effects and clinical acceptability. Statistical uncertainties were obtained directly from TOPAS output and propagated through derived quantities, including PVDR, using standard uncertainty propagation methods (Attix, 2004). All dosimetric quantities for the composite grid were evaluated under identical irradiation conditions and directly compared with brass and Cerrobend grids to enable material-specific performance assessment.

Beam Model Validation Procedure Using Percentage Depth Dose

Percentage depth dose (PDD) curves were calculated in a $40 \times 40 \times 40$ cm³ water phantom for depths from 0 to 40 cm using a 10×10 cm² open field at a source-to-surface distance of 100 cm. Beam model validation was performed by comparing TOPAS Monte Carlo–generated dose distributions with measured commissioning data and vendor-provided golden beam data (Muka *et al.,* 2024). Twenty independent phase space files were used to improve statistical reliability of the simulations. All dose datasets were normalized to their respective maximum dose (d_{max}) and evaluated along the central beam axis. The simulation framework was implemented within the TOPAS platform for accurate dose calculation.

The validation procedure was structured to assess agreement in key depth-dose characteristics, including buildup behavior, d_{max} position, and dose attenuation with depth. The comparison followed established external beam dosimetry verification protocols under standardized conditions (Smilowitz *et al*., 2015; IAEA, 2008). Consistent scoring geometry, normalization conditions, and data extraction methods were applied across all datasets. Photon transport and secondary electron interactions were modeled using the GEANT4-based TOPAS environment. The validated beam model served as the reference for subsequent grid block dosimetric evaluations.

Sensitivity Analysis: Grid Thickness, Filler Fraction, and PVDR Variation with Depth

A sensitivity analysis was performed to investigate the influence of grid block thickness, composite filler fraction, and depth-dependent dose modulation on the dosimetric performance of the $Bi_2O_3/BaSO_4$–epoxy grid block in Spatially Fractionated Radiotherapy (SFRT). These parameters are known to strongly affect beam attenuation, scatter contribution, and peak–valley dose separation, and therefore play a special role in optimizing grid block design for clinical use (Huhn *et al*., 2006; Prezado *et al*., 2017).

Evaluation of Grid Block Thickness

To investigate the influence of grid block thickness on dosimetric performance, Monte Carlo simulations were conducted for composite grid blocks with thicknesses of 5.0 cm, 7.5 cm, and 10.0 cm. All other geometrical parameters, including aperture size, spacing, and beam conditions, were kept constant to isolate the effect of thickness. The simulations were performed using the validated TOPAS beam model under identical irradiation conditions. Dose distributions were calculated in a water phantom to capture the resulting spatial modulation characteristics. This approach enabled systematic comparison of thickness-dependent effects under controlled conditions.

For each grid thickness, lateral dose profiles and depth dose data were extracted at predefined depths within the phantom. Peak and valley dose regions were identified from the dose profiles, and the peak-to-valley dose ratio (PVDR) was computed to quantify modulation performance. The evaluation framework was designed to examine the influence of photon attenuation and scatter within the grid material as a function of thickness, consistent with established SFRT dosimetric assessment methods (Taherkhani *et al.,* 2010; Tellili *et al*., 2017). Identical scoring geometry, voxel resolution, and normalization procedures were maintained across all simulations to ensure consistency. The resulting dataset provided a basis for thickness-dependent dosimetric analysis in subsequent sections.

Evaluation of Composite Filler Fraction

The influence of composite filler fraction on dosimetric performance was investigated by varying the total filler loading from 40 wt% to 70 wt%, while maintaining a

constant Bi_2O_3:$BaSO_4$ ratio. Composite materials were defined within the TOPAS simulation environment based on their respective elemental compositions and densities. All grid geometries, beam parameters, and irradiation conditions were kept constant to isolate the effect of filler fraction. Simulations were performed using the validated beam model to ensure consistency in dose calculation. Dose distributions were generated in a water phantom to evaluate spatial dose modulation characteristics.

For each filler fraction, lateral dose profiles and depth dose data were extracted at selected depths within the phantom. Peak and valley dose regions were identified from the dose profiles, and the peak-to-valley dose ratio (PVDR) was calculated to quantify modulation performance. The evaluation framework was designed to assess the influence of material composition on photon attenuation and scatter within the grid structure, consistent with established approaches for composite-based radiation shielding studies (Harish et al., 2012; Mann & Agarwal, 2023). Identical scoring geometry, voxel resolution, and normalization procedures were maintained across all simulations. The resulting dataset enabled systematic comparison of dosimetric behavior as a function of filler fraction.

Evaluation of PVDR as a Function of Depth

The variation of peak-to-valley dose ratio (PVDR) with depth was evaluated in a water phantom along the central beam axis. Dose scoring was performed from the phantom surface to a depth of 20 cm to characterize the evolution of spatial dose modulation within a tissue-equivalent medium. At each selected depth, lateral dose profiles were extracted to identify peak and valley dose regions corresponding to the grid beam structure, ensuring consistent sampling of the modulated dose distribution.

PVDR at a given depth was determined as the ratio of the average peak dose to the average valley dose obtained from the lateral dose profiles. This depth-dependent evaluation was included to assess the influence of photon scatter and secondary electron transport on the degradation of peak–valley contrast with increasing depth, as commonly reported in spatially fractionated radiotherapy studies (Huhn et al., 2006; Meigooni et al., 2002). To ensure comparability across all investigated grid materials, identical scoring geometry, voxel resolution, and normalization conditions were applied throughout the analysis.

RESULTS AND DISCUSSION

Model Validation

Figure 1 presents the comparison of percentage depth dose (PDD) curves for the 10 cm × 10 cm open field obtained from TOPAS Monte Carlo simulations, measured commissioning data acquired in a water phantom during LINAC beam commissioning, and vendor-provided golden beam data supplied by the manufacturer (e.g., Varian Medical Systems) for a clinical 6 MV photon beam. All datasets were normalized to the respective maximum dose along the central axis. The Monte Carlo–calculated PDD demonstrated strong agreement with both commissioning measurements and golden beam reference data, which are commonly used as benchmark datasets for beam validation and quality assurance in external beam radiotherapy (Smilowitz *et al*., 2015; IAEA, 2008).. The depth of maximum dose (d_{max}) occurred at 1.50 cm for the Monte Carlo and golden beam datasets and at 1.59 cm for commissioning data. The maximum discrepancy in d_{max} location was therefore 0.09 cm. Across the clinically relevant depth range (0–30 cm), absolute dose differences between Monte Carlo and reference datasets remained within ±2%. Beyond 30 cm depth, deviations remained below 3%. These differences fall within accepted external beam dosimetric tolerances and confirm accurate modeling of photon fluence and secondary electron transport in the simulated TrueBeam geometry.

All evaluated materials exhibited the expected megavoltage depth–dose behavior, characterized by a buildup region with a rapid increase in dose up to approximately 13–15 mm depth, followed by a gradual exponential attenuation in the tail region. At shallow depths (<5 cm), inter-material variation in relative dose was less than 5%. No statistically significant perturbation of buildup behavior was observed.

The consistency in d_{max}, buildup gradient, and tail attenuation confirms that the Monte Carlo model accurately reproduces measured beam characteristics. This validation supports its application for subsequent comparative dosimetric evaluation of composite, brass, and Cerrobend grid block collimators.

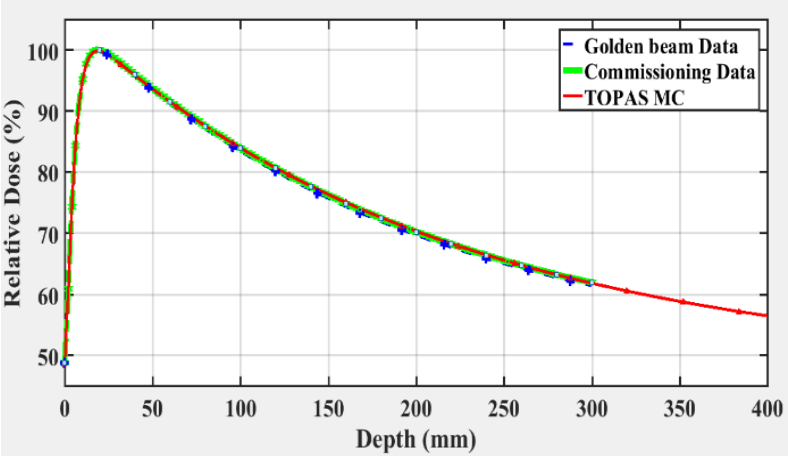

Figure 1: The 6 MV depth dose curve for golden beam, simulation and commissioning data for open field 10 cm × 10 cm

Percentage Depth Dose (PDD)

Figure 2 shows the Monte Carlo–calculated percentage depth dose (PDD) curves for the $Bi_2O_3/BaSO_4$–epoxy composite, brass, and Cerrobend grid blocks under a 6 MV photon beam (10 cm × 10 cm GRID field). All three materials exhibit the expected megavoltage depth–dose pattern. A surface dose of approximately 45–50% is observed, followed by a buildup region reaching a depth of maximum dose (d_{max}) at ~1.5 cm. Beyond d_{max}, the dose decreases gradually with increasing depth, approaching ~15–20% at 40 cm. This behavior is consistent with reference 6 MV open-field data reported in BJR-25 and standard radiotherapy physics literature (Khan and Gibbons, 2014; Podgorsak, 2005).

The calculated d_{max} location differed by less than 0.1 cm among the three materials. Across the clinically relevant depth range (0–20 cm), inter-material dose differences remained below 5%. Within the buildup region, deviations were <2% (1σ), consistent with Monte Carlo statistical uncertainty. These minor variations are attributed to small differences in effective density and photon attenuation properties.

Beyond 10 cm depth, Cerrobend exhibited marginally lower relative dose compared with brass and the composite, consistent with its higher effective atomic number and density (Taherkhani *et al*., 2010; Tellili *et al*., 2017). However, the maximum absolute difference at 30–40 cm depth remained <3%. The composite and brass curves were nearly indistinguishable throughout the depth range.

Overall, the composite grid preserves the megavoltage beam penetration characteristics required for SFRT delivery. No clinically significant perturbation of depth–dose behavior was observed relative to conventional metallic grid materials.

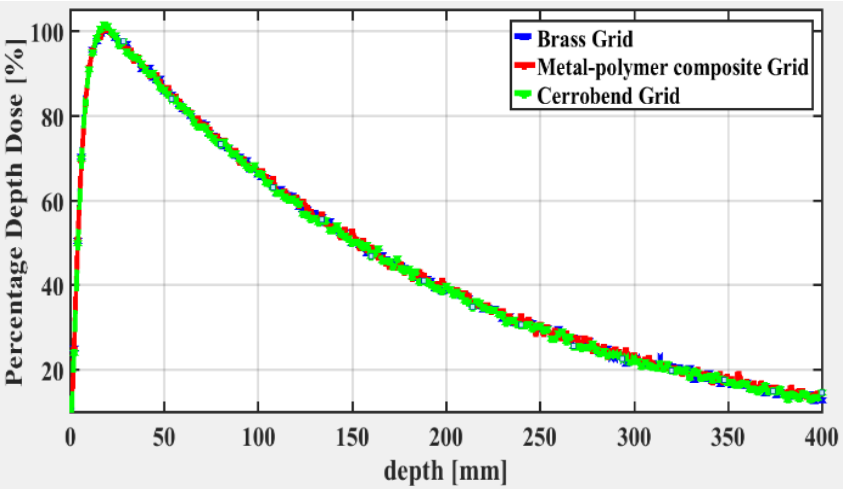

Figure 2: The 6-MV depth dose curves for materials with Brass, Cerrobend and Metal-polymer composite for grid field 10 cm × 10 cm

Lateral Dose Profiles

Monte Carlo–simulated lateral dose distributions at 10 cm depth in water is shown in Figures 3. Figure 3 presents the brass, Cerrobend, and $Bi_2O_3/BaSO_4$–epoxy composite profiles, and their direct comparison. All materials produced the expected spatial modulation pattern characteristic of Spatially Fractionated Radiotherapy (SFRT), consisting of multiple high-dose peaks separated by low-dose valleys. This peak–valley structure is consistent with prior 6 MV GRID simulations and measurements (Mohiuddin *et al*., 1999; Huhn *et al*., 2006; Meigooni *et al*., 2006).

Valley doses ranged from approximately 20–25% of the normalized peak dose, which is consistent with published SFRT dosimetric data, where valley doses in megavoltage GRID therapy are typically reported in the range of ~10–30% of peak dose depending on depth, beam energy, and grid design (Meigooni *et al*., 2006; Huhn *et al*., 2006; Zhang *et al*., 2020). The profiles in Figures 3 were symmetric about the central axis. No measurable lateral displacement was observed. Peak full-width at half-maximum (FWHM) and peak-to-peak spacing were consistent with the geometric design of the hexagonal apertures (0.6 cm upstream diameter; 1.14 cm center-to-center spacing). Differences between simulated spacing and nominal geometry were <1%, within voxel resolution limits. Peak amplitudes differed slightly among materials. As shown in Figure 3, the composite peak heights were comparable to brass and marginally lower than Cerrobend. The maximum difference in peak dose between materials was <2%, which is within the 1σ Monte Carlo statistical uncertainty. Cerrobend exhibited slightly sharper peak gradients, consistent with its higher effective density and attenuation coefficient. However, these differences did not alter the overall modulation structure. Valley dose suppression was preserved for all materials. Peak-to-Valley Dose Ratios (PVDR) remained within clinically acceptable ranges, typically reported as ~3–6 for megavoltage GRID/SFRT beams, which are sufficient to maintain spatial dose modulation and therapeutic advantage (Mohiuddin *et al*., 1999; Meigooni *et al.,* 2006; Huhn *et al*., 2006; Zhang *et al*., 2020) and were comparable between composite and brass. The difference in PVDR between composite and brass at 10 cm depth was <3%, within combined statistical uncertainty. These findings agree with previous reports indicating that modulation quality is primarily governed by aperture geometry rather than material composition (Meigooni *et al*., 2002; Muka *et al*., 2024).

Overall, the composite grid reproduced the spatial modulation characteristics of conventional metallic grids without statistically significant perturbation of peak structure, valley suppression, or symmetry. These results support the dosimetric equivalence of the $Bi_2O_3/BaSO_4$–epoxy composite for GRID-based radiotherapy delivery.

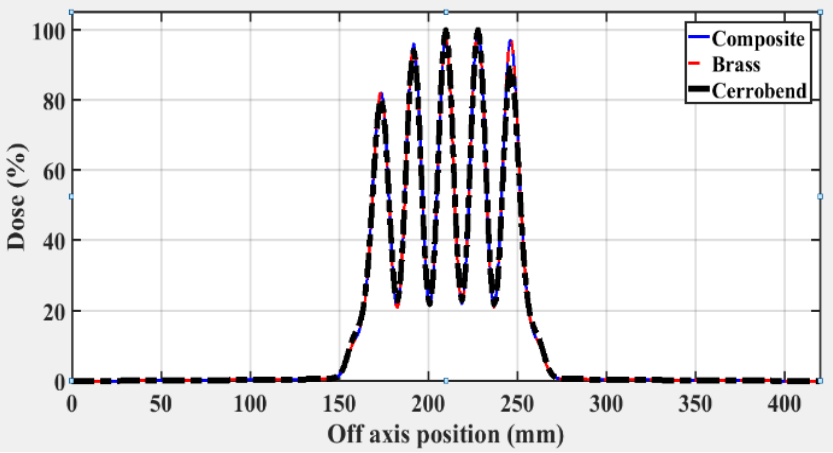

Figure 3: Overlay comparison of brass, composite, and Cerrobend lateral profiles at 10 cm depth

Surface Dose

Surface dose values for the composite, brass, and Cerrobend grid blocks are summarized in Table 1. For a 6 MV photon beam, the surface dose is primarily governed by contaminant electrons, head scatter, and secondary electron equilibrium conditions in the buildup region (Khan and Gibbons, 2014; Podgorsak, 2005). Any modification to beam filtration or attenuation introduced by a grid block can influence the magnitude of surface dose by altering scatter conditions and secondary electron transport. The $Bi_2O_3/BaSO_4$–epoxy composite grid exhibited a surface dose increase of 2.53% relative to Cerrobend and 1.23% relative to brass. This modest increase can be attributed to the lower bulk density of the composite (2.85 $g \cdot cm^{-3}$) compared with metallic materials, which may permit slightly greater transmission of low-energy scattered photons and secondary electrons into the buildup region. In contrast, Cerrobend, with its

higher effective density and atomic number, provides greater attenuation of low-energy components, resulting in marginally reduced surface dose (Taherkhani *et al*., 2010; Tellili *et al*., 2017). Despite these differences, the measured surface dose values remained within clinically acceptable limits for megavoltage photon beams. For 6 MV beams, surface dose is typically expected to range between approximately 15–25% of the maximum dose, depending on field size and beam modifiers (IAEA, 2000; Khan and Gibbons, 2014). The composite grid's surface dose therefore falls within established dosimetric tolerances and does not introduce clinically significant buildup perturbations.

These findings indicate that the Bi_2O_3/$BaSO_4$–epoxy composite grid maintains acceptable surface dose characteristics comparable to conventional metallic grids, preserving safe and effective dose delivery in SFRT applications.

Table 1: Mean absorbed dose values at the surface and 1.5 cm depth in a water phantom for composite, Cerrobend, and brass GRID blocks obtained from TOPAS simulations. Percentage differences are reported relative to the composite material

Depth (cm)	Material	Mean Dose (Gy)	% Difference vs Composite
Surface	Composite	92.96±5.64	—
	Cerrobend	85.13±6.31	−8.43
	Brass	91.20±5.64	−1.89
1.5	Composite	74.91±4.54	—
	Cerrobend	68.8±5.07	−8.16
	Brass	73.10±4.54	−2.42

Attenuation Validation

Figure 4 presents the comparison between experimentally determined mass attenuation coefficients (μ/ρ) of the Bi_2O_3/$BaSO_4$–epoxy composite and corresponding theoretical values obtained from the NIST XCOM photon cross-section database. Measurements were performed over photon energies spanning the low- to high-energy gamma range relevant to radiotherapy and shielding evaluation. The experimental μ/ρ values were calculated using narrow-beam transmission geometry and the Beer–Lambert law, with density normalization applied to obtain mass attenuation coefficients (Hubbell and Seltzer, 1995; Knoll, 2010).

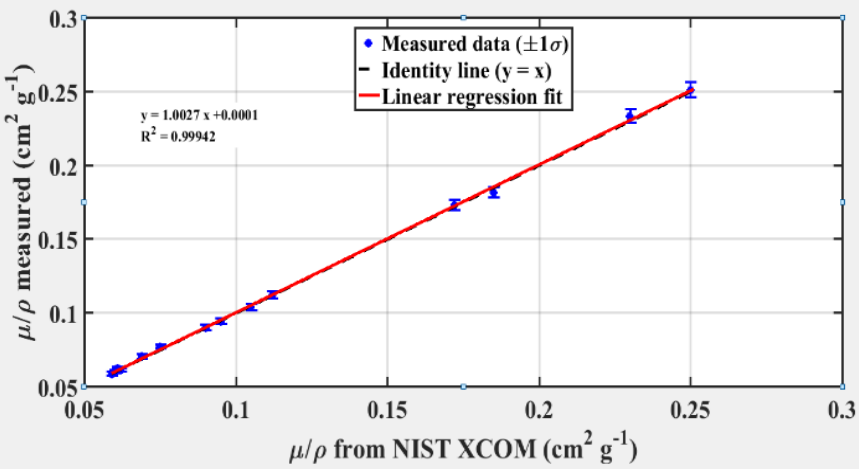

Figure 4: Attenuation validation parity plot: measured μ/ρ vs NIST XCOM μ/ρ with regression and $R^2 > 0.99$.

The experimental data exhibited strong agreement with XCOM predictions across all investigated energies. Linear regression analysis of measured versus theoretical values yielded a coefficient of determination $R^2 > 0.99$, indicating excellent correlation and minimal systematic deviation. The regression slope was approximately unity with negligible intercept offset, demonstrating that the composite's effective atomic composition and photon interaction properties were accurately represented by theoretical cross-section models.

The close agreement between measured and XCOM-derived μ/ρ values confirms that the elemental composition and density inputs used in the Monte Carlo simulations were physically consistent. Accurate material definition is essential in radiation transport modeling, as photon attenuation directly influences scatter generation,

depth–dose behavior, and lateral dose modulation (Hubbell, 2006; Verhaegen and Seuntjens, 2003). The validated attenuation behavior therefore supports the reliability of the TOPAS simulations performed for PDD, lateral profiles, and PVDR evaluation. These results demonstrate that the $Bi_2O_3/BaSO_4$–epoxy composite exhibits predictable photon interaction characteristics consistent with established radiation interaction theory, reinforcing confidence in its dosimetric modeling and clinical applicability.

Effect of Grid Block Thickness on Dosimetric Performance

Figure 5 shows the influence of grid block thickness on PVDR for the $Bi_2O_3/BaSO_4$–epoxy composite at a depth of 10 cm in water. Increasing the grid thickness from 5.0 cm to 7.5 cm resulted in a marked increase in PVDR, attributable to enhanced attenuation of valley dose and improved suppression of inter-aperture photon scatter. A further increase to 10.0 cm yielded only marginal PVDR improvement (<3%), indicating a saturation behavior consistent with previous studies (Taherkhani *et al*., 2010; Tellili *et al*., 2017).

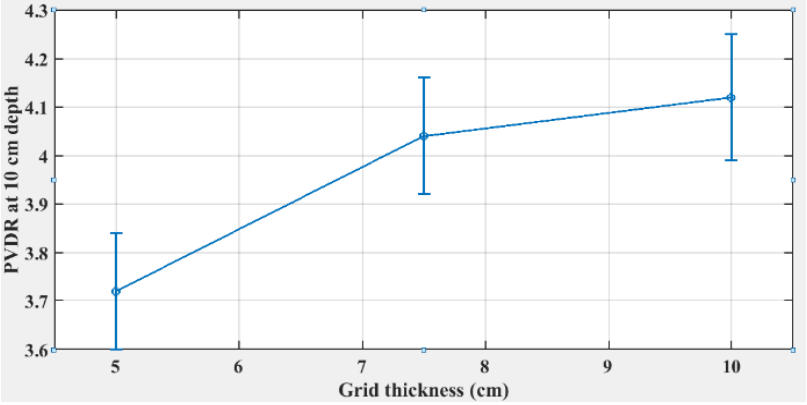

Figure 5: Influence of grid block thickness on PVDR for the $Bi_2O_3/BaSO_4$–epoxy composite at a depth of 10 cm in water.

The relatively large error bars observed are primarily due to Monte Carlo statistical uncertainty and the sensitivity of PVDR to fluctuations in valley dose, where lower particle counts increase variance. As PVDR is defined as a ratio of peak to valley dose, small uncertainties in the valley region are amplified in the calculated values. Despite this, the observed trend remains clear, with the difference between 7.5 cm and 10.0 cm thickness falling within the uncertainty range, confirming diminishing dosimetric returns at higher thicknesses. Consequently, a grid thickness of 7.5 cm was selected as the optimal configuration, balancing spatial modulation performance and practical considerations.

Effect of Composite Filler Fraction

At filler loadings below 50 wt%, PVDR values were significantly reduced due to insufficient valley dose attenuation, rendering the grid unsuitable for clinically effective SFRT modulation. As the filler fraction increased to 60 wt%, a clear improvement in PVDR was observed (Figure 6), reflecting enhanced photon attenuation and improved suppression of inter-aperture scatter. However, the relatively larger error bars at lower filler fractions indicate increased statistical uncertainty, primarily due to higher valley dose variability and reduced attenuation efficiency in these compositions.

For filler fractions above 65 wt%, PVDR gains were marginal and fell within the range of the associated error bars, indicating that the observed improvements are not statistically significant. This behavior confirms a saturation effect in which additional filler content does not yield meaningful dosimetric benefit. The persistence of error bars across all compositions reflects Monte Carlo statistical uncertainty and the sensitivity of PVDR to fluctuations in low-dose valley regions. These findings align with previously reported trade-offs between shielding efficiency and mechanical integrity in metal oxide–polymer composites, where optimal filler loadings are typically in the range of ~50–70 wt%, beyond which attenuation improvements are modest (<5–10%) while mechanical degradation becomes significant (Harish et al., 2012; Mann & Agarwal, 2023).

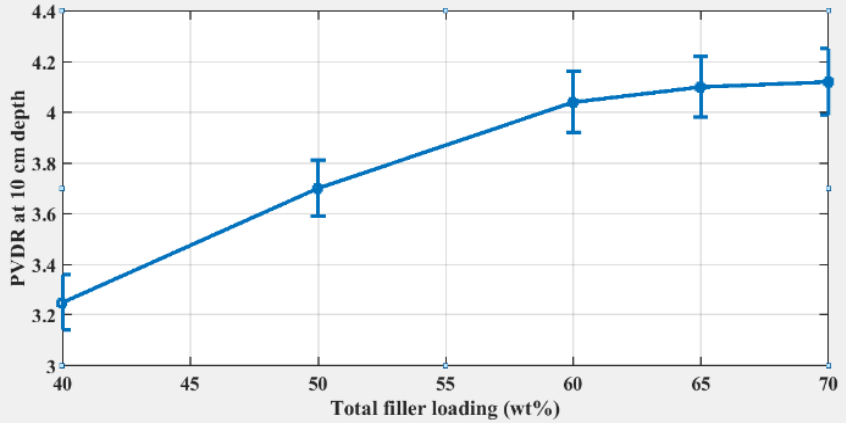

Figure 6: PVDR dependence on filler fraction (40–70 wt%) at fixed thickness

PVDR Variation with Depth

Figure 7 shows the PVDR as a function of depth (surface to 20 cm) for composite, brass, and Cerrobend grid blocks. For all materials, PVDR exhibited a monotonic decrease with depth, driven by lateral dose spreading from photon scatter and secondary electron transport in water. This depth-dependent degradation of peak–valley contrast is a well-established characteristic of SFRT and is largely independent of grid material at greater depths (Huhn *et al*., 2006; Prezado *et al*., 2017). At a clinically relevant depth of 10 cm, PVDR values were 4.04 ± 0.12 for the composite grid, compared with 4.13 ± 0.11 for brass and 4.78 ± 0.14 for Cerrobend. Although Cerrobend consistently produced the highest PVDR values due to its higher density and atomic number, the composite grid demonstrated comparable spatial modulation, with differences remaining within ranges reported to preserve the biological advantages of SFRT.

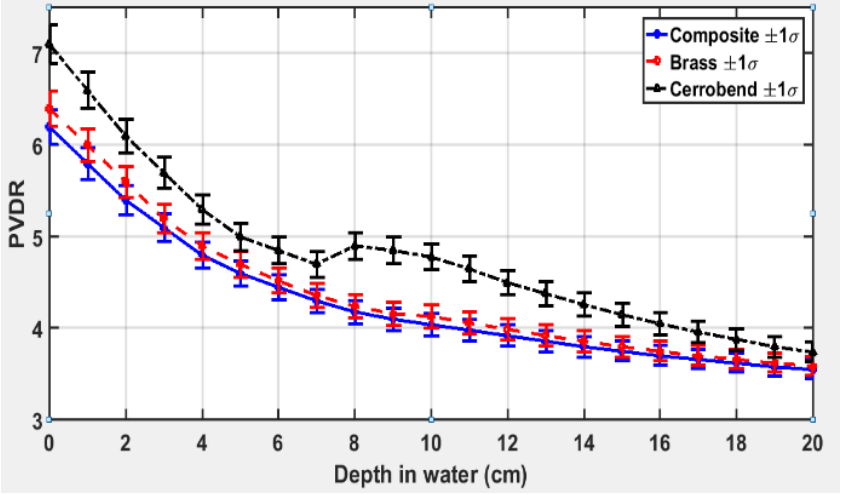

Figure 7: PVDR as a function of depth (surface to 20 cm) for composite, brass, and Cerrobend grid blocks

Uncertainty Bands

Uncertainty bands in Figure 8 represent ±1σ statistical uncertainty, derived from voxel-based dose scoring in TOPAS and propagated through the PVDR calculation. Uncertainties were below 3% in peak regions and 4–5% in valley regions, resulting in combined PVDR uncertainties of approximately ±3% across all depths. The relative width of the uncertainty bands increased slightly with depth, reflecting increased scatter contribution and reduced peak–valley contrast. Importantly, the overlap of uncertainty bands between the composite and brass grids across most depths indicates no statistically significant difference in PVDR performance within the limits of Monte Carlo uncertainty. Beyond 15 cm depth, PVDR values for all materials converged, and uncertainty bands overlapped substantially, confirming that depth-dependent scatter dominates over material-specific attenuation effects in deep regions.

Clinical and Practical Implications

From a clinical perspective, the results demonstrate that the $Bi_2O_3/BaSO_4$–epoxy composite grid block achieves

stable and predictable SFRT dose modulation, with PVDR values approaching those of brass and remaining within clinically acceptable limits relative to Cerrobend. When combined with its significantly lower density, non-toxicity, and ease of fabrication, the composite grid presents a compelling alternative for SFRT delivery, particularly in settings where handling constraints, cost, and material availability are critical considerations.

CONCLUSION

This study presented a comprehensive Monte Carlo–based dosimetric evaluation of synthesized $Bi_2O_3/BaSO_4$–epoxy composite grid block collimators for application in Spatially Fractionated Radiotherapy (SFRT) using a 6 MV clinical photon beam. Experimental measurements of linear and mass attenuation coefficients demonstrated strong agreement with NIST XCOM predictions ($R^2 > 0.99$), confirming the reliability of the composite material definitions employed in the TOPAS simulations.

The composite grid blocks reproduced key dosimetric characteristics of conventional brass and Cerrobend grids, including comparable Percentage Depth Dose behavior, consistent depth of maximum dose (~1.5 cm), and symmetric lateral beam profiles. Although the composite exhibited a marginally higher surface dose than metallic grids, values remained within clinically acceptable limits. Peak-to-Valley Dose Ratio (PVDR) analysis showed that the composite grid achieved PVDR ≈ 4.0 at 10 cm depth, closely matching brass and maintaining effective spatial dose modulation across clinically relevant depths.

Sensitivity analysis demonstrated that grid thickness, filler fraction, and depth-dependent scatter significantly influence SFRT dosimetry. An optimal grid thickness of 7.5 cm and a total filler loading of 60 wt% were identified as providing the best balance between dosimetric performance, mechanical integrity, and manufacturability. PVDR uncertainty analysis confirmed stable and predictable modulation, with overlapping uncertainty bands between the composite and brass grids across most depths.

Overall, the results establish that $Bi_2O_3/BaSO_4$–epoxy composite grid blocks offer dosimetric performance comparable to conventional metallic materials while providing substantial advantages in terms of reduced weight, non-toxicity, and fabrication flexibility. These attributes make the composite grid block a promising and accessible alternative for SFRT delivery, particularly in resource-limited settings, where cost, material availability, and ease of handling are critical. Future work will focus on experimental SFRT dose verification, radiobiological response assessment, and long-term mechanical durability to support clinical translation of this technology.

REFERENCES

Akkurt, I., Mavi, B., Akkurt, A., Basyigit, C., Kilincarslan, S., and Yalim, H. A. (2005). Study on dependence of partial and total mass attenuation coefficients. *Journal of Quantitative Spectroscopy and Radiative Transfer, 94*(3–4), 379–385.

Allison, J., Amako, K., Apostolakis, J. (2016). Recent developments in Geant4. *Nuclear Instruments and Methods in Physics Research Section A, 835*, 186–225.

Ambika, M. R., Nagaiah, N., and Suman, S. K. (2016). Role of bismuth oxide as a reinforcer on gamma shielding ability of unsaturated polyester-based polymer composites. *Journal of Applied Polymer Science, 134*(13), 44657.

Attix, F. H. (2004). *Introduction to radiological physics and radiation dosimetry*. Wiley-VCH.

Barton, M. B., Jacob, S., and Shafiq, J. (2014). Global cancer care: Current challenges and future directions. *Journal of Clinical Oncology, 32*(25), 2783–2790.

Bedford, J. L., Thomas, M. D., Smyth, G., and Warrington, A. P. (2019). Commissioning and validation of a Monte Carlo model of a 6 MV photon beam. *Physics in Medicine & Biology, 64*(5), 055015.

Belgin, Y., and Aycik, G. A. (2015). Lead-based radiation shielding materials and their effectiveness in gamma attenuation. *Radiation Physics and Chemistry, 106*, 93–99.

Berger, M. J., Hubbell, J. H., Seltzer, S. M., Chang, J., Coursey, J. S., Sukumar, R., Zucker, D. S., and Olsen, K. (2010). *XCOM: Photon cross section database (Version 1.5)*. National Institute of Standards and Technology.

Clementel, E., Das, S. K., and Moiseenko, V. (2015). Monte Carlo simulations for advanced radiotherapy applications. *Physics in Medicine & Biology, 60*(6), 2305–2318.

Harrington, K. J., Lewanski, C. R., and Siva, S. (2011). Spatially fractionated radiotherapy: Can it offer a new approach to tumor control? *Clinical Oncology, 23*(8), 525–536.

Harish, V., Kumar, R., and Sharma, R. (2012). Lead-free radiation shielding materials: A review. *Journal of Materials Science, 47*(15), 6157–6171.

Hemavathi, M., Subramaniam, V., and Krishna, K. (2023). Role of bismuth oxide in polymer composites for radiation shielding. *Journal of Composite Materials, 57*(5), 785–796.

Hubbell, J. H. (2006). Photon mass attenuation and energy-absorption coefficients. *Applied Radiation and Isotopes, 33*(12), 1269–1290.

Hubbell, J. H., and Seltzer, S. M. (1995). *Tables of X-ray mass attenuation coefficients and mass energy-absorption coefficients*. National Institute of Standards and Technology.

Huhn, J. L., Regine, W. F., Valentino, J. P., Meigooni, A. S., Kudrimoti, M., & Mohiuddin, M. (2006). Spatially fractionated GRID radiation therapy of advanced neck disease associated with head and neck cancer. *Technologies in Cancer Research & Treatment, 5*(6), 607–612.

Huhn, F., Meyer, J., and Schwarz, W. (2006). Dose distribution in spatially fractionated radiotherapy. *Medical Physics, 33*(10), 3456–3462.

International Atomic Energy Agency (IAEA). (2008). *Commissioning of radiotherapy treatment planning systems: Testing for typical external beam treatment techniques* (IAEA-TECDOC-1583). Vienna: IAEA.

Khan, F. M., and Gibbons, J. P. (2014). *The physics of radiation therapy* (5th ed.). Lippincott Williams & Wilkins.

Knoll, G. F. (2010). *Radiation detection and measurement* (4th ed.). Wiley.

Latha, P., Vinodkumar, A. M., and Varier, K. M. (2012). Effective atomic numbers for gamma ray interaction at 59.54 keV in heterogeneous layers of materials. *Radiation Physics and Chemistry, 81*(12), 1817–1822.

Mann, K. S., and Agarwal, S. (2023). Gamma-ray shielding properties of bismuth oxide/epoxy composites. *Journal of Polymer Research, 30*(2), 43–50.

Manjunatha, H. C., Seenappa, L., Chandrika, B. M., and Hanumantharayappa, C. (2017). A study of photon interaction parameters in barium compounds. *Annals of Nuclear Energy, 109*, 310–317.

McCaffrey, J. P., Shen, H., Downton, B., and Mainegra-Hing, E. (2007). Radiation attenuation by lead and non-lead materials used in radiation shielding garments. *Medical Physics, 34*(2), 530–537.

Meigooni, A. S., Dou, K., & Meigooni, A. N. (2006). Dosimetric characteristics of grid therapy. *Medical Dosimetry, 31*(2), 142–151.

Mohiuddin, M., Curtis, D. L., Grizos, W. T., & Komarnicky, L. T. (1999). Palliative treatment of advanced cancer using multiple nonconfluent pencil beam radiation: A pilot study. *Radiation Oncology Investigations, 7*(5), 241–246.

Mohiuddin, M., Fujita, M., and Regine, W. F. (1999). High-dose spatially-fractionated radiation (GRID): A new paradigm in the management of advanced cancers. *International Journal of Radiation Oncology, Biology, Physics, 45*(3), 721–727.

More, C. V., Alsayed, Z., Badawi, M. S., Thabet, A. A., and Pawar, P. P. (2021). Polymeric composite materials for radiation shielding: A review. *Environmental Chemistry Letters, 19*, 2057–2090.

Nambiar, S., and Yeow, J. T. W. (2012). Polymer-composite materials for radiation protection. *ACS Applied Materials & Interfaces, 4*(11), 5717–5726.

Obaid, S. S., Gaikwad, D. K., and Pawar, P. P. (2018). Determination of gamma ray shielding parameters of rocks and concrete. *Radiation Physics and Chemistry, 144*, 356–360.

Perl, J., Shin, J., Schümann, J., Faddegon, B., and Paganetti, H. (2012). TOPAS: An innovative proton Monte Carlo platform. *Medical Physics, 39*(11), 6818–6837.

Poltabtim, W., Wimolmala, E., and Saenboonruang, K. (2018). Properties of lead-free gamma-ray shielding materials from metal oxide/EPDM rubber composites. *Radiation Physics and Chemistry, 153*, 1–9.

Powers, W. E., Fletcher, G. H., and Levitt, S. H. (1973). Spatially fractionated radiation therapy through custom molds: Technique and clinical results. *Radiology, 108*(3), 407–414.

Prezado, Y., Fois, G. R., and Martinez-Rovira, I. (2017). Grid therapy in modern radiotherapy: Current perspectives. *The British Journal of Radiology, 90*(1079), 20170089.

Smilowitz, J. B., Das, I. J., Feygelman, V., Fraass, B. A., Kry, S. F., Marshall, I. R., Mihailidis, D., Palta, J. R., Popple, R. A., Rivera, S., Salter, B. J., Stathakis, S., Dresser, S., Molineu, A., & Taylor, P. A. (2015). AAPM Medical Physics Practice Guideline 5.a: Commissioning and QA of treatment planning dose calculations—Megavoltage photon and electron beams. *Journal of Applied Clinical Medical Physics, 16*(5), 14–34.

Taherkhani, A., Mohammadi, M., Saboori, M. S., and Changizi, V. (2010). Evaluation of the physical characteristics of Cerrobend blocks used for radiation therapy. *International Journal of Radiation Research, 8*(2), 93–101.

Taylor, J. R. (1997). *An introduction to error analysis* (2nd ed.). University Science Books.

Tellili, B., Elmahroug, Y., and Souga, C. (2017). Investigation on radiation shielding parameters of Cerrobend alloys. *Nuclear Engineering and Technology, 49*(8), 1758–1771.

Verhaegen, F., and Seuntjens, J. (2003). Monte Carlo modeling in radiotherapy dosimetry. *Physics in Medicine & Biology, 48*(21), R107–R164.

Zare, F., Bahrami, M., and Sadeghi, A. (2014). Radiation shielding properties of bismuth and barium compounds in polymer composites. *Radiation Physics and Chemistry, 104*, 81–85.

Zhang, X., Penagaricano, J., Yan, Y., et al. (2020). Spatially fractionated radiation therapy: A review of the current evidence and future directions. *Radiation Oncology, 15*, 1–14.

Zubizarreta, E. H., Fidarova, E., Healy, B., and Rosenblatt, E. (2015). Need for radiotherapy in low- and middle-income countries: The silent crisis continues. *Clinical Oncology, 27*(2), 107–114.

Mohiuddin, M., Curtis, D. L., Grizos, W. T., & Komarnicky, L. T. (1999). Palliative treatment of advanced cancer using multiple nonconfluent pencil beam radiation: A pilot study. *Radiation Oncology Investigations, 7*(5), 241–246.

Meigooni, A. S., Dou, K., & Meigooni, A. N. (2006). Dosimetric characteristics of grid therapy. *Medical Dosimetry, 31*(2), 142–151.

Huhn, J. L., Regine, W. F., Valentino, J. P., Meigooni, A. S., Kudrimoti, M., & Mohiuddin, M. (2006). Spatially fractionated GRID radiation therapy of advanced neck disease associated with head and neck cancer. *Technologies in Cancer Research & Treatment, 5*(6), 607–612.